Acta Crystallographica Section F
Structural Biology and Crystallization Communications
ISSN 1744-3091

Neutron diffraction studies towards deciphering the protonation state of catalytic residues in the bacterial KDN9P phosphatase

Tyrel Bryan,[a]‡ Javier M. González,[b]‡ John P. Bacik,[b] Nicholas J. DeNunzio,[c] Clifford J. Unkefer,[b] Tobias E. Schrader,[d] Andreas Ostermann,[e] Debra Dunaway-Mariano,[a] Karen N. Allen[c] and S. Zoë Fisher[b]*

[a]Department of Chemistry and Chemical Biology, University of New Mexico, Albuquerque, NM 87131, USA, [b]BioScience Division B-11, Los Alamos National Laboratory, PO Box 1663, Los Alamos, NM 87545, USA, [c]Department of Chemistry, Boston University, 590 Commonwealth Avenue, Boston, MA 02115, USA, [d]Jülich Centre for Neutron Science (JCNS) at Heinz Maier-Leibnitz Zentrum (MLZ), Forschungszentrum Jülich GmbH, Lichtenbergstrasse 1, 85748 Garching, Germany, and [e]Heinz Maier-Leibnitz Zentrum (MLZ), Technische Universität München, Lichtenbergstrasse 1, 85748 Garching, Germany

‡ These authors contributed equally to this manuscript.

Correspondence e-mail: zfisher@lanl.gov

Received 1 July 2013
Accepted 31 July 2013

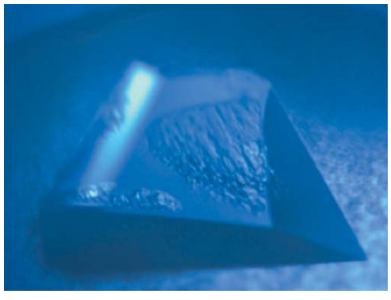

The enzyme 2-keto-3-deoxy-9-*O*-phosphononononic acid phosphatase (KDN9P phosphatase) functions in the pathway for the production of 2-keto-3-deoxy-D-*glycero*-D-*galacto*-nononic acid, a sialic acid that is important for the survival of commensal bacteria in the human intestine. The enzyme is a member of the haloalkanoate dehalogenase superfamily and represents a good model for the active-site protonation state of family members. Crystals of approximate dimensions 1.5 × 1.0 × 1.0 mm were obtained in space group $P2_12_12$, with unit-cell parameters a = 83.1, b = 108.9, c = 75.7 Å. A complete neutron data set was collected from a medium-sized H/D-exchanged crystal at BIODIFF at the Heinz Maier-Leibnitz Zentrum (MLZ), Garching, Germany in 18 d. Initial refinement to 2.3 Å resolution using only neutron data showed significant density for catalytically important residues.

1. Introduction

The haloalkanoate dehalogenase superfamily of enzymes (HADSF) is represented in the proteomes of organisms from all three domains of life, wherein its members participate in numerous diverse biological processes (Collet *et al.*, 1998; Koonin & Tatusov, 1994). The superfamily is largely made up of phosphatases (Allen & Dunaway-Mariano, 2004), which conserve a Rossmann-fold catalytic domain consisting of a three-layered α/β sandwich of repeating β–α units. The accessorizing of the core Rossmann domain with inserted domains or segments has allowed diversification towards substrates and provides a natural division of the HADSF into three major structural classes (C0, C1 and C2) based on the location and topology of the insert (Burroughs *et al.*, 2006). HADSF phosphatase biochemical functions have been invented and reinvented across these structural classes (Burroughs *et al.*, 2006). One critical function taken on by the HADSF is in the synthesis of polyhydroxylated α-keto acids that are integrated into glycoproteins and glycolipids for cell-surface display in prokaryotes and eukaryotes (Angata & Varki, 2002). A rare but important polyhydroxylated α-keto acid, 2-keto-3-deoxy-D-*glycero*-D-*galacto*-nononic acid (KDN), is formed through the action of a phosphatase, 2-keto-3-deoxy-9-*O*-phosphononononic acid phosphatase (KDN9PP), which is a prototypical member of the YbrI clade of the HADSF C0 subfamily (Burroughs *et al.*, 2006). The presence of the KDN unit on the bacterial outer cell membrane enables mimicry of the human epithelial cell polysialic acid to aid in survival and foraging of commensal bacteria within the intestine (Coyne & Comstock, 2008).

In the YbrI clade, the biological unit is comprised of four identical Rossmann-fold core subunits that oligomerize *via* a central β-barrel domain formed from the inserts from each subunit such that residues from the adjacent Rossmann domain contribute to the active site of the neighboring subunit (with four active sites per tetramer; Parsons *et al.*, 2002). Substrates bind through the phosphoryl group at the Rossmann core domain, with the substrate leaving group forming interactions with the adjacent subunit. The core-domain catalytic scaffold is formed by four loops (Fig. 1) that contribute one or more amino-acid side chains to participate in binding the substrate phosphoryl group and/or the Mg^{2+} ion (Wang *et al.*, 2008; Lu *et al.*, 2009). Loop 1 positions the Asp nucleophile (Asp10 in KDN9PP) and the

Asp acid/base catalyst (Asp12). Both aspartate residues also bind the Mg^{2+} cofactor *via* the Asp10 nucleophile carboxylate group and the Asp12 backbone C═O. The substrate phosphoryl group coordinates to the Mg^{2+} cofactor and engages in hydrogen-bond interactions with the side chains of the conserved Ser/Thr of Loop 2 (Thr54) and Lys of Loop 3 (Lys80). Loop 4 provides a coordination bond from Asp103, increasing the affinity for Mg^{2+}. Through the use of this scaffold, phosphoryl transfer is catalyzed in two partial reactions: phosphoryl transfer from the substrate to the Asp nucleophile and phosphoryl transfer from the aspartylphosphate intermediate to a water molecule (Baker *et al.*, 1998). The aspartate general acid/base residue functions to protonate the substrate leaving group in the first partial reaction and to deprotonate the water nucleophile in the second partial reaction (Lahiri *et al.*, 2002).

Despite the availability of high-resolution X-ray crystal structures of KDN9PP, there are still many unknowns regarding the active-site protonation and the catalytic mechanism of this diverse class of enzymes. Knowledge of the protonation states of the conserved catalytic residues and hydrogen-bonding interactions in the active site will allow in-depth understanding of the mechanistic strategy used by the HADSF in catalyzing the formation and hydrolysis of the aspartylphosphate intermediate. Although the general acid/base aspartate residue is hypothesized to be the proton donor to the substrate leaving group, in most HADSF phosphatases this residue is thought to form a hydrogen bond to a positively charged residue such as Lys30 (Fig. 1*b*; Lu *et al.*, 2005). The optimal pH for catalysis in HADSF phosphatases typically falls in the pH 6.0–7.0 range. The aspartate general acid/base may be protonated in the unliganded form of the enzyme (its pK_a may be perturbed upwards from that of aspartate in solution), or it may be that the active form of the substrate is singly protonated (the second pK_a of α-glucose-6-phosphate is 6.2; Knight *et al.*, 1986) and that upon binding the proton transfers from the substrate phosphate group to the aspartate.

As a representative of the HADSF, KDN9PP is a candidate for neutron studies (i) because of the availability of high-resolution (∼1.1 Å) X-ray crystal structures of apo and transition-state analog complexes (Wang *et al.*, 2008; Lu *et al.*, 2009), (ii) because it uses

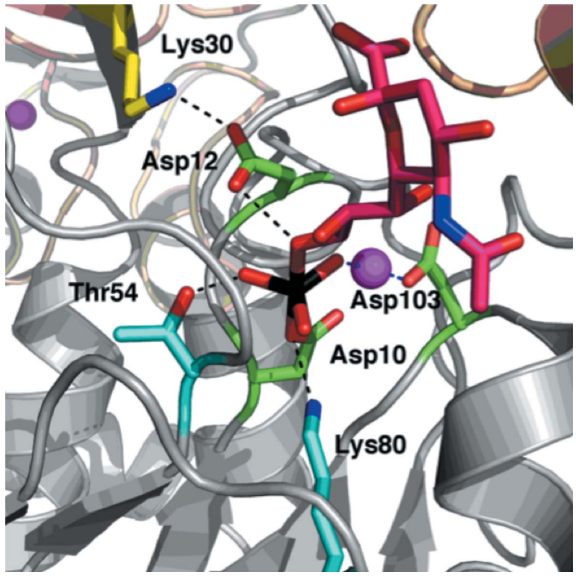

Figure 1
Active site of the KDN9PP–Mg^{2+}–VO_3^-–neuramic acid complex with the ligands and catalytic residues shown in stick representation and the Mg^{2+} cofactor shown as a magenta sphere. The X-ray coordinates are from Lu *et al.* (2009).

Table 1
Room-temperature neutron data-collection statistics.

Values in parentheses are for the highest resolution shell. The X-ray data shown are from a hydrogenous crystal.

	BIODIFF neutron data	In-house X-ray data
No. of images	201	180
Wavelength (Å)	2.66	1.54
Space group	$P2_12_12$	$P2_12_12$
Unit-cell parameters (Å, °)	a = 83.1, b = 108.9, c = 75.7, $\alpha = \beta = \gamma$ = 90.0	a = 82.7, b = 108.9, c = 75.6, $\alpha = \beta = \gamma$ = 90.0
Unit-cell volume (Å^3)	685570	682339
Resolution (Å)	44.0–2.30 (2.37–2.30)	36.3–1.78 (1.81–1.78)
No. of reflections (total/unique)	56137/28420 (1796)	463685/66613 (3697)
Multiplicity	2.0 (1.4)	7.0 (6.6)
Mean $I/\sigma(I)$	4.6 (1.1)	14.5 (3.4)
R_{merge}† (%)	0.14 (0.520)	0.070 (0.554)
$R_{p.i.m.}$‡ (%)	0.11 (0.478)	0.029 (0.232)
Completeness (%)	91.4 (70.6)	99.9 (98.3)

† $R_{merge} = \sum_{hkl}\sum_i |I_i(hkl) - \langle I(hkl)\rangle| / \sum_{hkl}\sum_i I_i(hkl)$. ‡ $R_{p.i.m.} = \sum_{hkl}\{1/[N(hkl) - 1]\}^{1/2} \sum_i |I_i(hkl) - \langle I(hkl)\rangle| / \sum_{hkl}\sum_i I_i(hkl)$.

oligomerization to close the active site and thus does not occur in open and closed forms caused by domain–domain movement that could complicate analysis and (iii) because it is amenable to crystallization at a range of pH values (pH 5.5–8.5), enabling studies of the protonation states of active-site residues and estimation of their pK_a (Wang *et al.*, 2008).

The position of hydrogen is essential to the understanding of catalysis, protein folding, ligand/drug/substrate binding and protein engineering (Blakeley *et al.*, 2008), yet it must often be surmised from indirect evidence. X-rays scatter from electron clouds with an increase in the magnitude of scattering occurring as a function of atomic number Z; thus, there is little to no information on H atoms. In contrast, neutrons scatter from atomic nuclei and scattering is similar in magnitude for all elements, making the assignment of H (or D) atom locations at medium resolution possible (Meilleur *et al.*, 2006; Blakeley *et al.*, 2008; Yokoyama *et al.*, 2012). A common strategy to overcome the negative scattering and large incoherent cross-section of H in neutron diffraction is H/D exchange. This dramatically improves the signal-to-noise ratio; therefore, H/D exchange is routinely used for crystal preparation prior to data collection (Chen *et al.*, 2012; Fisher, Kovalevsky, Domsic, Mustyakimov, McKenna *et al.*, 2010). A great deal of information can be extracted from a neutron crystal structure of H/D-exchanged samples, such as solvent accessibility, levels of H/D exchange, thermal fluctuations and identification of minimal folding domains in proteins (Bennett *et al.*, 2008; Fisher, Kovalevsky, Domsic, Mustyakimov, Silverman *et al.* 2010; Yokoyama *et al.*, 2012). Compared with the spherical solvent peaks in electron-density maps, the shape of solvent nuclear density maps makes it possible to differentiate between OH^-, H_3O^+ and H_2O (or OD^-, D_3O^+ and D_2O) species (Kovalevsky *et al.*, 2011; Cuypers *et al.*, 2013). Similarly, H/D atoms on amino-acid side chains are visible and help to determine their protonation status and hydrogen-bonding interactions (Fisher *et al.*, 2011; Kovalevsky, Fisher *et al.*, 2010; Kovalevsky, Hanson *et al.*, 2010; Ahmed *et al.*, 2007). X-ray and neutron diffraction data are highly complementary and can be combined during model refinement in a joint approach. This leads to more accurate structures and is the only approach that can give direct atomic information on H/D-atom positions to guide enzyme mechanistic studies (Adams *et al.*, 2009; Afonine *et al.*, 2010).

To gain insight into the KDN9PP active-site structure and catalytic mechanism, we initiated joint X-ray and neutron diffraction studies of H/D-exchanged KDN9PP at the Protein Crystallography Station

(PCS) at Los Alamos Neutron Science Center. Crystal preparation and feasibility studies were carried out at the PCS and support laboratories. The full data set reported here (Table 1) was collected on the BIODIFF instrument at the FRM II research reactor in Germany. Here, we report the crystal preparation and data collection for the first neutron diffraction experiment on a HADSF member, KDN9PP.

2. Experimental

2.1. Protein expression, purification and crystallization of KDN9PP for neutron studies

Recombinant wild-type KDN9PP was isolated from transformed and induced *Escherichia coli* cells and purified to homogeneity as described previously (Wang *et al.*, 2008) with the following modifications. Notably, a tenfold increase in yield was obtained by the use of Terrific Broth plus glycerol with growth to high OD_{600} before induction, as described below. Also, optimization of the flow rates used for the hydrophobic affinity column led to improved purification of the protein. *E. coli* BL21 (DE3) pLysS cells were transformed with recombinant KDN9PP pET-3a plasmid. The transformed cells were grown at 310 K with agitation at 250 rev min^{-1} in Terrific Broth (Life Technologies) containing 4 ml glycerol per litre of TB and 50 µg ml^{-1} ampicillin for 4–6 h to an OD_{600} of ∼0.6–1.0. At this stage, protein expression was induced overnight at 290 K with 0.4 m*M* isopropyl *β*-D-1-thiogalactopyranoside. The cells were harvested by centrifugation (6500 rev min^{-1}) for 10 min at 277 K to yield 10 g of wet cells per litre of culture medium. The cell pellet (40 g) was suspended in 400 ml ice-cold buffer *A* (50 m*M* Na HEPES pH 7.5) and lysed using a French press. The cell lysate was centrifuged at 277 K for 20 min at 20 000 rev min^{-1}. The supernatant protein was fractioned by ammonium sulfate-induced precipitation. The 50–90%(*w*/*v*) ammonium sulfate fraction was collected by centrifugation at 20 000 rev min^{-1} for 15 min. The pellet was dissolved in 30 ml buffer *B* [50 m*M* Na HEPES, 16%(*w*/*v*) ammonium sulfate pH 7.5]. The resuspended protein was loaded onto a 10 × 300 mm BS Sepharose column (GE Life Sciences) pre-equilibrated with buffer *B* at 277 K. The column was washed with 5 CV (column volumes) of buffer *B* and the protein was eluted with a linear gradient (10 CV) of 100–0% buffer *B* (16–0% ammonium sulfate). The column fractions were analyzed by SDS–PAGE. The desired protein fractions (90–100% buffer *A*) were collected and concentrated using 10 kDa molecular-weight cutoff Amicon Ultra centrifugal filters. The protein sample was then subjected to buffer exchange using a HiPrep 16/60 Sephacryl S-200 column equilibrated with 10 m*M* Na HEPES pH 7.0. The protein was >99% pure as judged by SDS–PAGE analysis and the total yield was ∼25 mg protein per gram of wet cells.

Purified KDN9PP was concentrated to 20 mg ml^{-1} prior to crystallization. Screening conditions were based on those previously published (Lu *et al.*, 2009) and refined to 0.1 *M* Tris–HCl pH 8.5, 0.2 *M* sodium acetate, 10 m*M* $MgCl_2$, 30%(*w*/*v*) PEG 4000 (Fig. 2). We first optimized the crystal-growth conditions in 24-well Linbro plates using both hanging and sitting drops. Drop sizes ranged from 10 to 40 µl. Once these conditions had been optimized, we used crystals from these drops to macroseed much larger drops (100–200 µl). For the large-drop setups, we used the Sandwich Box from Hampton Research. The crystallization drops were set up in the nine-well glass plate and were allowed to undergo vapor diffusion against 25 ml well solution. Several large single crystals (∼1.0–1.5 mm in any one dimension) deemed to be suitable for neutron diffraction studies were selected and mounted in thick-walled quartz capillaries (0.4 mm thickness Vitrotubes from Vitrocom). Once mounted, the crystals were wicked dry and a liquid plug of ∼150 µl perdeuterated well solution [0.1 *M* Tris–HCl, 0.2 *M* sodium acetate, 10 m*M* $MgCl_2$, 30%(*w*/*v*) PEG 4K in 99.9% pure D_2O] was introduced on either side of the crystal prior to sealing the capillary with beeswax. The crystals were allowed to undergo vapor H/D exchange in the capillary for 1–2 weeks prior to neutron diffraction testing. The first series of tests were conducted at the PCS instrument at LANSCE (Fig. 3*a*). The full data collection reported here was completed at BIODIFF at FRM II, Technische Universität München (TUM), Germany (Fig. 3*b*).

The crystals used for X-ray structure determination were grown using the same conditions but with much smaller volumes and using traditional 24-well plates. Specifically, the sitting-drop method was employed using 10 µl protein solution and 10 µl reservoir solution to give a 20 µl total drop size. Crystals appeared after only a few days and were mounted in 1 mm thin-walled quartz capillaries containing a plug of the deuterated buffer solution. Even though the H/D atoms do not contribute significantly to the X-ray scattering, there may be subtle chemical differences (hydrogen-bond lengths *etc.*) between hydrogenous (all-H) and exchanged (H/D) samples and it is desirable to keep the two data sets as isomorphous as possible. For the purpose of initial data refinement and assessment we used an all-hydrogenous crystal for room-temperature X-ray data collection. Crystallization, X-ray data collection and processing for the H/D-exchanged crystal are ongoing.

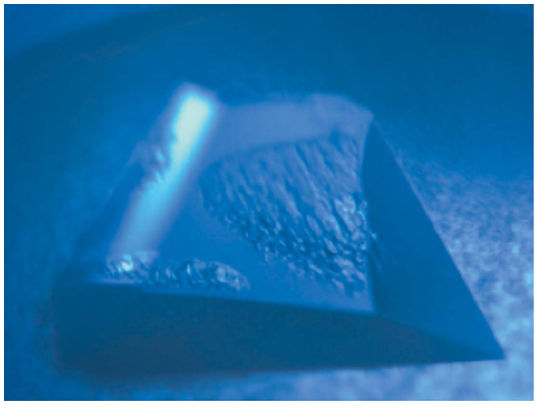

Figure 2
Photograph of an H/D-exchanged large single KDN9PP crystal grown at pH 8.5 (dimensions of ∼1.5 × 1.0 × 1.0 mm).

2.2. Room-temperature X-ray and neutron data collection and reduction

Suitable H/D-exchanged crystals of KDN9PP were selected for both room-temperature X-ray and neutron data collection. Neutron diffraction quality and data-collection feasibility were determined using the Protein Crystallography Station at LANSCE. Several 24 h test exposures were collected. These images were processed with a version of *d*TREK* that had been modified in-house for use with wavelength-resolved Laue neutron data (Pflugrath, 1999; Langan & Greene, 2004). Although these H/D-exchanged crystals did diffract, they were not deemed to be suitable for full data collection (Fig. 3*a*). This was most likely to be owing to the age of the samples. Subsequently, several fresh crystals were prepared, transported to BIODIFF at the FRM II, TUM, Germany and shown to diffract well enough to enable full data collection (Table 1; Fig. 3*b*).

Full neutron data collection was conducted at the monochromatic diffractometer BIODIFF with a cylindrical neutron image-plate

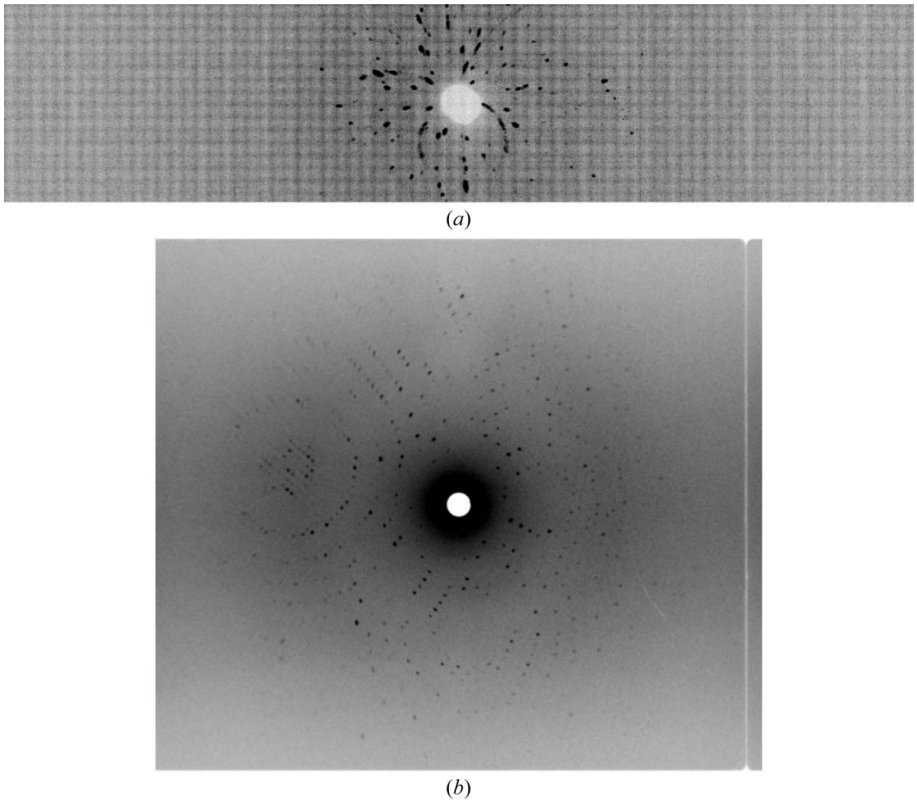

Figure 3
Representative neutron diffraction images collected from H/D-exchanged KDN9PP crystals. (*a*) Neutron Laue time-of-flight diffraction test image for KDN9PP collected at the Protein Crystallography Station at LANL and (*b*) monochromatic neutron diffraction pattern collected at BIODIFF at FRM II.

detector (Niimura *et al.*, 1994; Maatel, Voreppe, France). The cylindrical area detector of BIODIFF provides a large coverage of reciprocal space, thereby allowing a large number of Bragg reflections to be recorded simultaneously. The readout resolution of the image-plate scanner was set to 250 µm. The data set was collected at room temperature using a pyrolytic graphite monochromator (PG002) set at a wavelength of 2.66 Å. A total of 201 frames were recorded with a rotation range of 0.3° per frame and an exposure time of 120 min. The intensities of the reflections were integrated and scaled with *DENZO* (v.1.96.2) and *SCALEPACK* (v.1.98.2) (Otwinowski & Minor, 1997; Minor *et al.*, 2006).

X-ray data were collected from a hydrogenous crystal at room temperature using an in-house Rigaku MicroMax-007 high-flux home source equipped with VariMax optics and an R-AXIS IV^{++} image plate. The source used is a standard Cu rotating-anode generator operated at 40 kV and 30 mA. The crystal-to-detector distance was 150 mm, with 1° oscillation steps and 2 min exposure per frame. Data processing and integration was performed using *MOSFLM* (Leslie, 1992) and the data were scaled and merged using *SCALA* (Evans, 2006). The reflections were reindexed using *SFTOOLS* (B. Hazes, unpublished work). The X-ray data were collected to 1.78 Å resolution from 180 frames. The data-set statistics are shown in Table 1. The model, including metals and solvent, refined against the X-ray data alone was used in the joint refinement. The starting model for the X-ray refinement was PDB entry 3e8m (Lu *et al.*, 2009). The molecular graphics in Figs. 1 and 4 were generated in *PyMOL* (v.1.5.0.4; Schrödinger LLC).

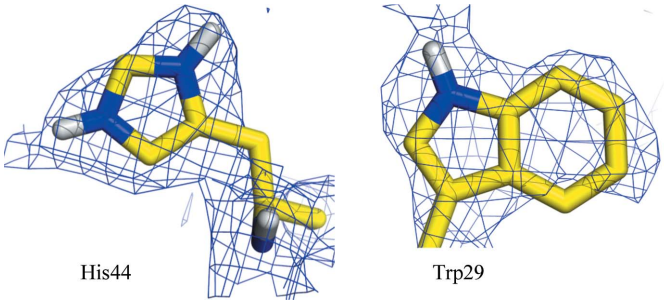

Figure 4
Representative nuclear density maps of His44 and Trp29 after rigid-body refinement against neutron data only. The exchanged D atoms are shown in white; $2F_o - F_c$ nuclear density is shown as a blue mesh and is contoured at 1σ.

3. Results and discussion

Several large KDN9PP crystals were prepared that were 1.0–1.5 mm in any one dimension. An H/D-exchanged KDN9PP crystal diffracted neutrons to 2.3 Å resolution and the final data set was ∼91% complete with an R_{merge} of 14% overall (Table 1). The preliminary neutron diffraction study of KDN9PP reported here is the first for an HADSF phosphatase and many of the results can be generalized to other HADSF phosphotransferases because of the conservation of the catalytic scaffold across family members. The large crystal size and the length of time that are required to acquire neutron data often deter most structural biologists from using neutron diffraction. These findings clearly demonstrate that it is feasible to obtain a complete neutron data set from a medium-sized H/D-exchanged crystal in 18 d. These data will reveal many important details about the KDN9PP active site and the ionization states of specific residues, as well as the hydrogen-bonding patterns in the active site that support catalysis.

After initial refinement using the neutron data alone, there was significant density for catalytically important residues (Fig. 4). Evidently His44 is protonated and fully H/D-exchanged, and the exchanged D on the side chain of Trp29 is clearly visible. Joint neutron and X-ray structure refinement is in progress using both a modified version of *CNS* for neutrons (*nCNS*) and *phenix.refine* (Adams *et al.*, 2009; Afonine *et al.*, 2010). Initial nuclear density maps after only one round of joint rigid-body refinement already reveal some of the details of protonation and hydrogen bonding in KDN9PP (Fig. 4). R_{work} and R_{free} (using *phenix.refine*) are already at 23.5 and 26.3%, respectively. We expect these values to improve as refinement continues and we will extend this analysis to other residues and solvent molecules. Analysis of the neutron structure will involve the detailed mapping of H atoms, water orientations and hydrogen bonding and analysis of active-site residues. These results will also guide planning for the next set of KDN9PP structures at a different pH and/or in complex with transition-state analogues.

We acknowledge funding from the National Institute of Health U54 GM093342 (to KNA and DD-M). The PCS is funded by the Department of Energy Office of Biological and Environmental Research (DOE-OBER).

References

Adams, P. D., Mustyakimov, M., Afonine, P. V. & Langan, P. (2009). *Acta Cryst.* D**65**, 567–573.

Afonine, P. V., Mustyakimov, M., Grosse-Kunstleve, R. W., Moriarty, N. W., Langan, P. & Adams, P. D. (2010). *Acta Cryst.* D**66**, 1153–1163.

Ahmed, H. U., Blakeley, M. P., Cianci, M., Cruickshank, D. W. J., Hubbard, J. A. & Helliwell, J. R. (2007). *Acta Cryst.* D**63**, 906–922.

Allen, K. N. & Dunaway-Mariano, D. (2004). *Trends Biochem. Sci.* **29**, 495–503.

Angata, T. & Varki, A. (2002). *Chem. Rev.* **102**, 439–469.

Baker, A. S., Ciocci, M. J., Metcalf, W. W., Kim, J., Babbitt, P. C., Wanner, B. L., Martin, B. M. & Dunaway-Mariano, D. (1998). *Biochemistry*, **37**, 9305–9315.

Bennett, B. C., Gardberg, A. S., Blair, M. D. & Dealwis, C. G. (2008). *Acta Cryst.* D**64**, 764–783.

Blakeley, M. P., Ruiz, F., Cachau, R., Hazemann, I., Meilleur, F., Mitschler, A., Ginell, S., Afonine, P., Ventura, O. N., Cousido-Siah, A., Haertlein, M., Joachimiak, A., Myles, D. & Podjarny, A. (2008). *Proc. Natl Acad. Sci. USA*, **105**, 1844–1848.

Burroughs, A. M., Allen, K. N., Dunaway-Mariano, D. & Aravind, L. (2006). *J. Mol. Biol.* **361**, 1003–1034.

Chen, J. C.-H., Hanson, B. L., Fisher, S. Z., Langan, P. & Kovalevsky, A. Y. (2012). *Proc. Natl Acad. Sci. USA*, **109**, 15301–15306.

Collet, J.-F., van Schaftingen, E. & Stroobant, V. (1998). *Trends Biochem. Sci.* **23**, 284.

Coyne, M. J. & Comstock, L. E. (2008). *J. Bacteriol.* **190**, 736–742.

Cuypers, M. G., Mason, S. A., Blakeley, M. P., Mitchell, E. P., Haertlein, M. & Forsyth, V. T. (2013). *Angew. Chem. Int. Ed.* **52**, 1022–1025.

Evans, P. (2006). *Acta Cryst.* D**62**, 72–82.

Fisher, S. Z., Kovalevsky, A., Domsic, J. F., Mustyakimov, M., McKenna, R., Silverman, D. N. & Langan, P. (2010). *Biochemistry*, **49**, 415–421.

Fisher, S. Z., Kovalevsky, A. Y., Domsic, J., Mustyakimov, M., Silverman, D. N., McKenna, R. & Langan, P. (2010). *Acta Cryst.* D**66**, 1178–1183.

Fisher, Z., Kovalevsky, A. Y., Mustyakimov, M., Silverman, D. N., McKenna, R. & Langan, P. (2011). *Biochemistry*, **50**, 9421–9423.

Knight, W. B., Weiss, P. M. & Cleland, W. W. (1986). *J. Am. Chem. Soc.* **108**, 2759–2761.

Koonin, E. V. & Tatusov, R. L. (1994). *J. Mol. Biol.* **244**, 125–132.

Kovalevsky, A., Fisher, Z., Johnson, H., Mustyakimov, M., Waltman, M. J. & Langan, P. (2010). *Acta Cryst.* D**66**, 1206–1212.

Kovalevsky, A. Y., Hanson, L., Fisher, S. Z., Mustyakimov, M., Mason, S. A., Forsyth, V. T., Blakeley, M. P., Keen, D. A., Wagner, T., Carrell, H. L., Katz, A. K., Glusker, J. P. & Langan, P. (2010). *Structure*, **18**, 688–699.

Kovalevsky, A. Y., Hanson, B. L., Mason, S. A., Yoshida, T., Fisher, S. Z., Mustyakimov, M., Forsyth, V. T., Blakeley, M. P., Keen, D. A. & Langan, P. (2011). *Angew. Chem. Int. Ed.* **50**, 7520–7523.

Lahiri, S. D., Zhang, G., Dunaway-Mariano, D. & Allen, K. N. (2002). *Biochemistry*, **41**, 8351–8359.

Langan, P. & Greene, G. (2004). *J. Appl. Cryst.* **37**, 253–257.

Leslie, A. G. W. (1992). *Jnt CCP4/ESF–EACBM Newsl. Protein Crystallogr.* **26**.

Lu, Z., Dunaway-Mariano, D. & Allen, K. N. (2005). *Biochemistry*, **44**, 8684–8696.

Lu, Z., Wang, L., Dunaway-Mariano, D. & Allen, K. N. (2009). *J. Biol. Chem.* **284**, 1224–1233.

Meilleur, F., Myles, D. A. A. & Blakeley, M. P. (2006). *Eur. Biophys. J.* **35**, 611–620.

Minor, W., Cymborowski, M., Otwinowski, Z. & Chruszcz, M. (2006). *Acta Cryst.* D**62**, 859–866.

Niimura, N., Karasawa, Y., Tanaka, I., Miyahara, J., Takahashi, K., Saito, H., Koizumi, S. & Hidaka, M. (1994). *Nucl. Instrum. Methods A*, **349**, 521–525.

Otwinowski, Z. & Minor, W. (1997). *Methods Enzymol.* **276**, 307–326.

Parsons, J. F., Lim, K., Tempczyk, A., Krajewski, W., Eisenstein, E. & Herzberg, O. (2002). *Proteins*, **46**, 393–404.

Pflugrath, J. W. (1999). *Acta Cryst.* D**55**, 1718–1725.

Wang, L., Lu, Z., Allen, K. N., Mariano, P. S. & Dunaway-Mariano, D. (2008). *Chem. Biol.* **15**, 893–897.

Yokoyama, T., Mizuguchi, M., Nabeshima, Y., Kusaka, K., Yamada, T., Hosoya, T., Ohhara, T., Kurihara, K., Tomoyori, K., Tanaka, I. & Niimura, N. (2012). *J. Struct. Biol.* **177**, 283–290